where C_{ij} is the central-axis term of the dose distribution of a broad beam that was obtained in a water phantom, including an inverse square correction. The variables $(\Delta x)_m$ and $(\Delta y)_m$ are the distances between the PB axis for the mth range bin and the calculation grid. For practical calculation, the deposited dose of each calculation grid may be calculated by integrating over the calculation grid size, and (10) may be rewritten as follows:

$$D(x,y) = \sum_{kl}\sum_{m=1}^{R_b} (N_{kl})_m (C_{kl})_m \cdot \frac{1}{2}\left[\mathrm{erf}\left(\frac{(\Delta x)_m + \frac{\delta_{xy}}{2}}{\sqrt{2\left(\overline{t^2}_{kl}\right)_m}}\right) - \mathrm{erf}\left(\frac{(\Delta x)_m - \frac{\delta_{xy}}{2}}{\sqrt{2\left(\overline{t^2}_{kl}\right)_m}}\right)\right] \times \frac{1}{2}\left[\mathrm{erf}\left(\frac{(\Delta y)_m + \frac{\delta_{xy}}{2}}{\sqrt{2\left(\overline{t^2}_{kl}\right)_m}}\right) - \mathrm{erf}\left(\frac{(\Delta y)_m - \frac{\delta_{xy}}{2}}{\sqrt{2\left(\overline{t^2}_{kl}\right)_m}}\right)\right]. \tag{11}$$

2.2. *Experimental geometry*

The AVF cyclotron at the National Cancer Centre East (NCCE), Japan, accelerates protons to 235 MeV (Nishio 1999, Tachikawa *et al* 1999). In this study, laterally uniform dose distributions were obtained by the double-ring dual-scattered method (Nishio *et al* 2006). The PBA (Hong *et al* 1996, Szymanowski *et al* 2001) and the PBRA were analysed by comparing the calculation results with the measured proton dose distributions in a heterogeneous slab phantom and an anthropomorphic phantom. The PBA and PBRA calculations were executed on a 2.8 GHz Quad Core Intel Xeon processor. A PTW 2D Array seven29^{TM} (PTW, Freiburg, Germany) was used as a proton dose detector (Spezi *et al* 2005, Hotta *et al* 2010). This 2D detector matrix has 729 uniformly arranged ionization chambers in a 1.0 cm pitch 27 × 27 array. The sensitive volume of a unit chamber is 0.5 cm × 0.5 cm × 0.5 cm. The ionization chambers of the array are open to the air. The offset thickness from the entrance surface to the centre of the sensitive volume is 0.8 cm in water-equivalent thickness. To compare the calculation results and measurements under the same conditions, the depth calculation was corrected by the offset thickness for calculating the dose distributions.

In the PBRA calculation, the width of the range bin for the redefinition procedure was set to 0.2 cm, which corresponded to the calculation grid size. The calculation results were convolved with a detector cell size of 0.5 cm × 0.5 cm. For practical use, we also accelerated the PBRA calculation by GPU implementation. We adopted the CUDA platform (NVIDIA, Driver Version 4.2) for the GPU implementation. The calculations used Quadro 4000, which has 256 processor cores with a core clock rate of 950 MHz, and were based on a Fermi architecture.

2.2.1. Heterogeneous slab phantom. As shown in figure 3, a heterogeneous slab phantom was used in the measurement to examine an extreme case of lateral heterogeneity in a human body.

Although this phantom geometry is not found clinically, the configurations may elucidate the effects of lateral density heterogeneity of protons on dose distributions (Kohno *et al* 2003, Kanematsu *et al* 2009b, Hotta *et al* 2010, Egashira *et al* 2012). Monoenergetic 190 MeV proton beams were used, and the lateral dose distributions were measured at depths of $z = -9.2$ cm, -0.8 cm, 4.2 cm, and 6.1 cm, with various polyethylene plate thicknesses. The air gap between the rectangular aperture of 10.0 cm × 10.0 cm and the phantom

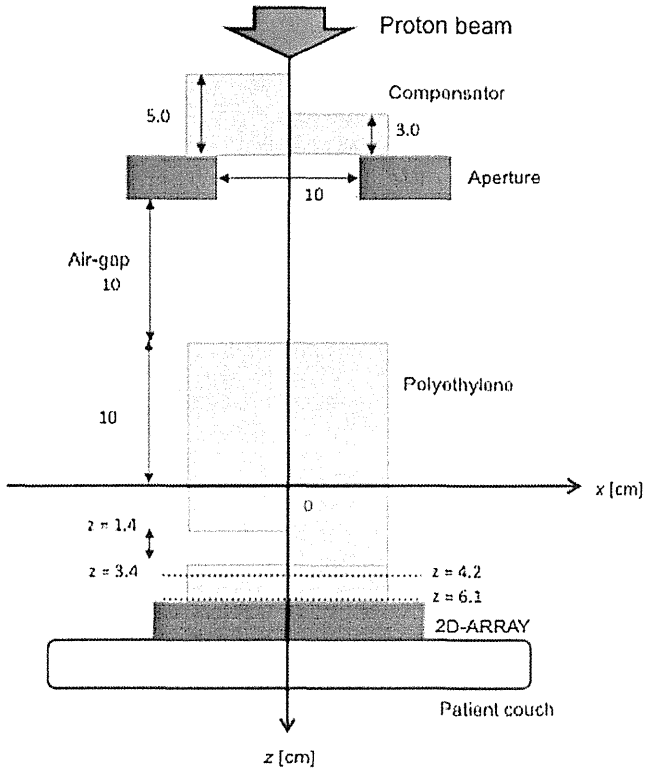

Figure 3. Experimental geometry for a heterogeneous slab phantom.

surface was fixed at 10.0 cm. The chamber pitch of 2D detector matrix we used was 1.0 cm. Since we were interested in the dose distribution close to the Bragg peak, the detector was shifted by 0.5 cm in the x direction to merge measurements with a lateral sampling pitch of 0.5 cm in the measurement at depths of $z = 4.2$ cm, and 6.1 cm. In the PBRA calculation, the interval of the redefinition planes was set equal to that of the calculation grids. For comparing the measurements and calculations, all of the dose data sets were normalized at a point ($x = -3.0$ cm, $y = 0.0$ cm, $z = -9.2$ cm) in the flat dose region. The computing time was monitored for the PBA and PBRA methods.

2.2.2. Anthropomorphic phantom. In the clinical situation, protons pass through complicated structures in the human body. To simulate the complicated arrangement of materials experienced in clinical applications, the head portion from a RANDO® phantom (Phantom Laboratory) was used. The calculated results were compared with measured data obtained by Hotta *et al* (2010). In this section, we briefly explain the experimental situation.

The anthropomorphic phantom mimics the density distribution in the human head by using resins with various compositions. Figure 4 shows the median sagittal and horizontal computed tomography (CT) images and the planning target volume (PTV) for this phantom, assuming a head and neck cancer with a volume of approximately 500 cm^3. The phantom was

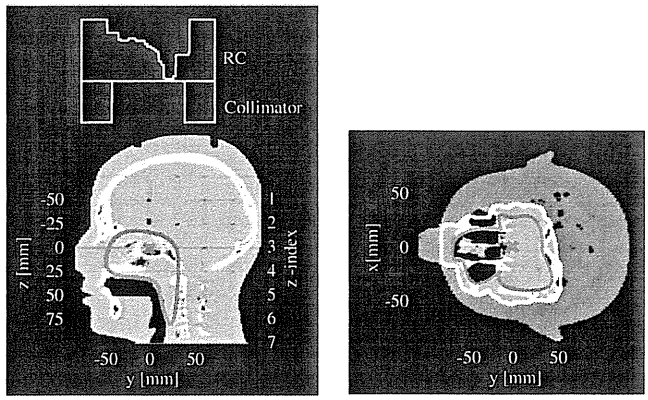

Figure 4. Experimental geometry for the anthropomorphic phantom measured by Hotta *et al* (2010).

composed of 2.5 cm thick horizontal layers. Dose distributions were measured in layers with Z-indices ranging from 1 to 7, which corresponded to $z = -50$ mm to $z = 100$ mm.

To simulate the clinical situation, the actual patient treatment procedure was performed, as follows: CT images were obtained, the PTV was delineated, the beam direction was determined, the corresponding range compensator and aperture collimator were manufactured, reference surface markers on the phantom were aligned with laser cross-hairs, and the phantom was irradiated on the patient couch. The smearing distance of the range compensator (Kooy *et al* 2008) was taken as 0.45 cm. A 235 MeV proton beam was modulated with a spread-out Bragg peak width of 6.0 cm, and a stack of phantom layers was mounted on the detector to measure the dose distribution in each measurement plane. The distance between the aperture collimator and the phantom entrance surface was fixed by adjusting the couch height. The reported results are the average of three measurements. All of the dose data sets were normalized with reference to the dose at the isocentre. The computing time was monitored for the PBA and PBRA methods.

3. Results

3.1. Heterogeneous slab phantom

The PBRA calculation was evaluated with the heterogeneity slab phantom. Figure 5 compares the depth- and lateral-dose profiles obtained from measurements and from the PBA and PBRA calculations.

As shown in figure 5(a), the main and overshot Bragg peaks appeared near depths of $z = 4$ cm and $z = 6$ cm, respectively. Lateral-dose profiles are shown in figures 5(b)–(e) at phantom depths of $z = -9.2$ cm, $z = -0.8$ cm, $z = 4.2$ cm and $z = 6.1$ cm, respectively. The PBRA was clearly superior to the conventional PBA in predicting the dose distribution in the region just distal to and shadowed by the edges of the inhomogeneity (air/polyethylene), particularly at the cold and hot spots. Although the magnitude of differences between the PBRA and measurements was as much as 2% at $z = 4.2$ cm, the geometry was very sensitive to misalignment of the density interface between the range compensator and the heterogeneous

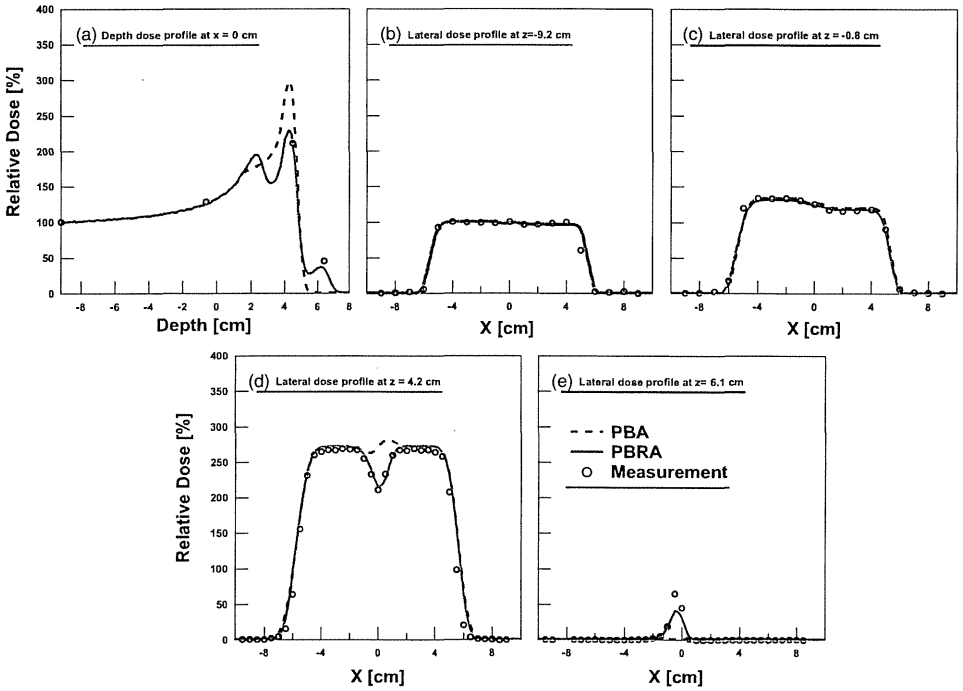

Figure 5. Depth- and lateral-dose distributions for the heterogeneous slab phantom.

slab in the phantom. The computational times for the PBA, PBRA and GPU-based PBRA calculations were 9.21, 60.2 and 30.1 s, respectively (see figure 8).

3.2. Anthropomorphic phantom

The PBRA calculation was evaluated with the anthropomorphic phantom. Figure 6 describes the isodose distributions in the coronal and sagittal planes at the isocentre obtained with the PBA calculation (left) and the PBRA calculation (right). The depth–dose distribution at $y = 0$ is also shown. The $Z = 6$ and $Z = 7$ planes were ignored because almost no protons reached these levels.

In the depth–dose profiles, discrepancies were observed between measurements and calculations and between the PBA and PBRA calculations. The discrepancy between measurements and calculations was caused by the range uncertainty of the phantom and the large dose gradient in the distal fall-off part of the Bragg curve. In the region that was deeper than $Z = 4$, where the protons reached the oral cavity, the difference between the PBA and PBRA calculations was more than 10%, due to differences in the path of the PB.

Figures 7(a) and (b) show the isodose distributions in the axial plane at the isocentre obtained with the PBA calculation (left), PBRA calculation (centre), and measurements (right) at $Z = 4$ and $Z = 5$. Lateral-dose profiles are also displayed in the figure, to illustrate some local differences.

The difference between the PBA and PBRA calculations arose from dose underestimations in the deep regions beyond air/tissue interface by the PBA, which disregarded the dose contributions of protons as they travelled through irregular paths along the phantom and reached the deep region. The distance to agreement (DTA) of the profiles around $x = 4$ cm

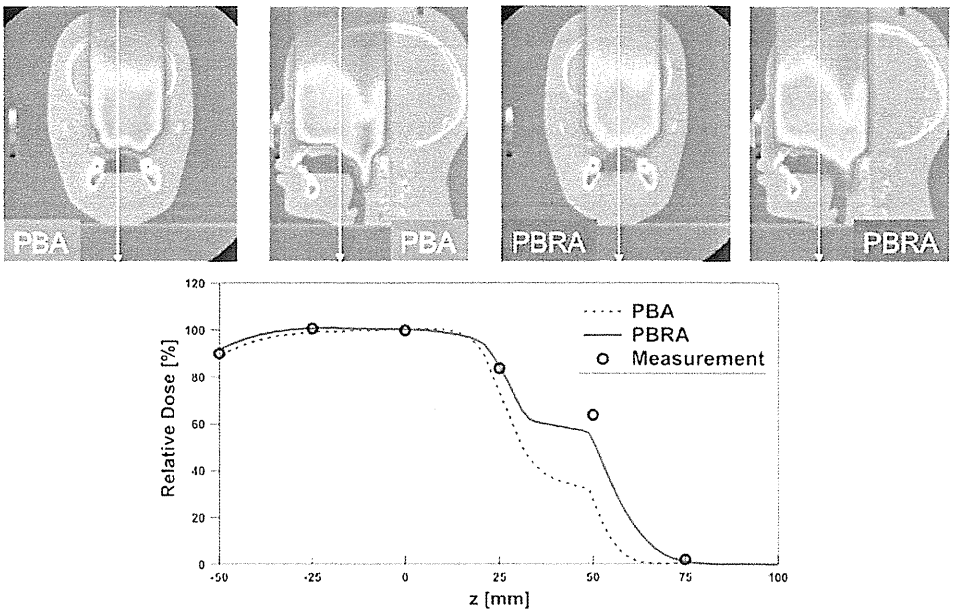

Figure 6. Isodose distributions in the coronal and sagittal planes and depth–dose distribution along the isocentre (arrow on the isodose distributions).

at $Z = 4$ and $y = 4$ cm at $Z = 5$, which were computed at a single point, were within 5 and 3 mm for the PBA and the PBRA calculations, respectively. The computational times for the PBA, PBRA and GPU-based PBRA calculations were 19.6, 272 and 59.0 s, respectively (see figure 8).

4. Discussion

This study addressed the use of the PBRA calculation in heterogeneous materials for proton therapy. Results calculated with the PBRA or PBA were compared with measured results in a heterogeneous slab phantom and an anthropomorphic phantom. The heterogeneous slab phantom simulated a simple geometry, in which an area of extreme lateral density heterogeneity was inserted. This set-up allowed us to investigate the effect of lateral density heterogeneity on the protons (Kohno *et al* 2003, Kanematsu *et al* 2009b, Hotta *et al* 2010, Egashira *et al* 2012). Behind the edges of the lateral density heterogeneity (i.e. air cavity), the dose was increased inside the edges and decreased outside, as more protons were scattered out by the polyethylene than were scattered in by the air cavity. The resulting detouring of the protons appeared as characteristic regions in the dose profiles.

Egashira *et al* (2012) reported that spatial resampling (i.e. beam redefinition) should be implemented immediately upstream of the lateral heterogeneity. Their resampling technique improved the accuracy of the PB calculation employing 1D density scaling because the number of the lateral heterogeneities in the compensator and phantom incidentally corresponded to the number of redefinition planes. As in Egashira *et al* (2012), we reconfirmed that use of the PBRA, in which the interval between and the number of redefinition planes may be arbitrary determined, also improved the accuracy of the proton PB calculation in this extreme geometry.

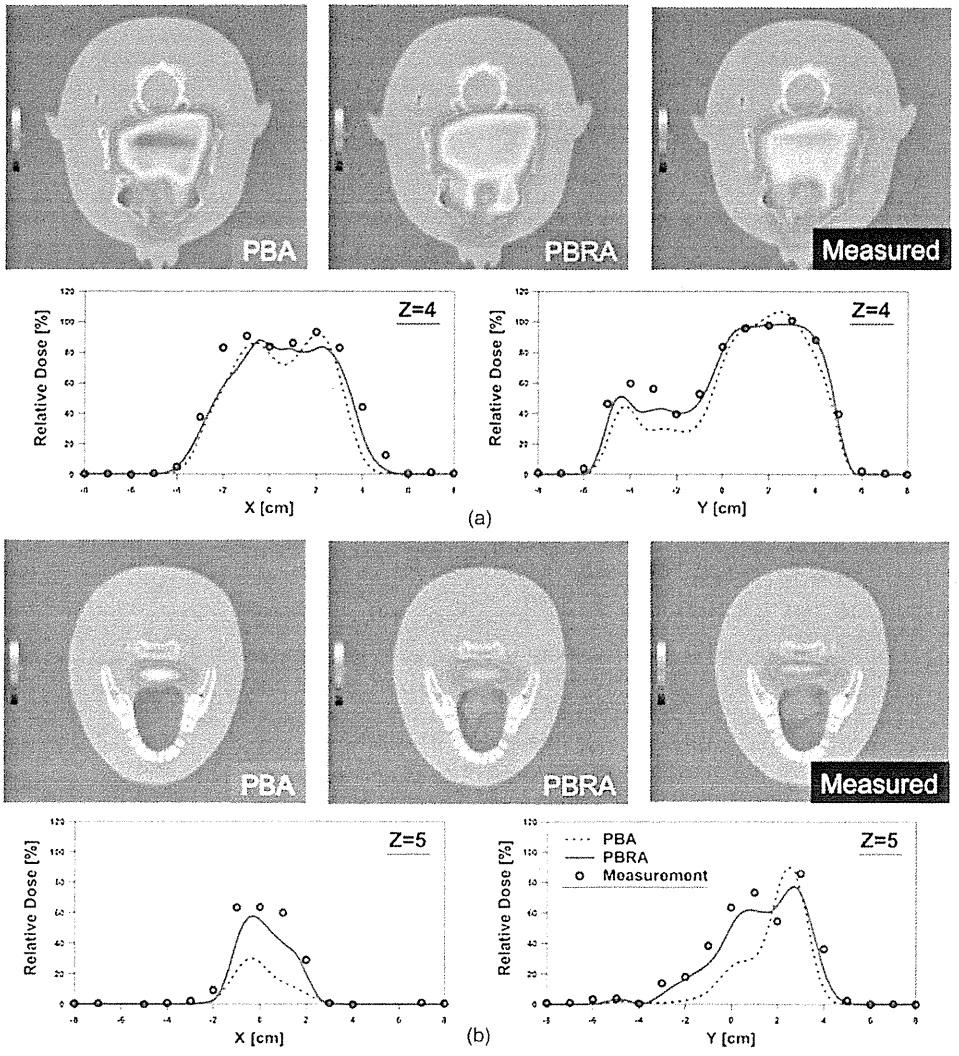

Figure 7. Isodose distributions in the axial plane and lateral-dose distribution in the x- and y-directions at (a) $Z = 4$ plane and (b) $Z = 5$ plane.

In clinical situations, protons pass through complicated structures, such as soft tissue, bone, and air, before they are stopped. To simulate this geometry, we used an anthropomorphic phantom with the measured data from Hotta *et al* (2010). In that previous study, the particles in the anthropomorphic phantom showed detouring effects due to multiple Coulomb scattering and nonstraight trajectories. The PBA disregarded the dose contributions of protons that travelled through irregular paths and reached the deep region and, therefore, underestimated the dose in the deep region (see figures 6 and 7). On the other hand, the redefined beams of the PBRA formed a detouring path that was different from PBs without redefinition, and the path of each redefined beam was straight. Consequently, the PBRA showed a dose increment

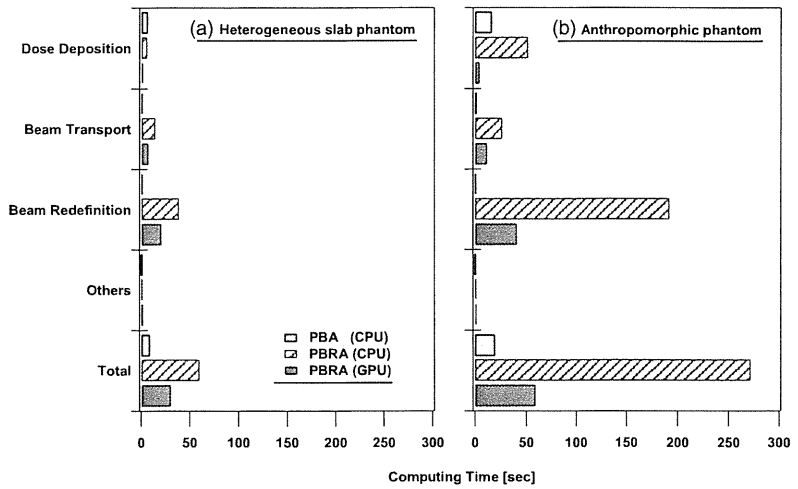

Figure 8. Performance of the PBA and PBRA calculations for the (a) heterogeneous slab phantom and (b) anthropomorphic phantom.

around depth $Z = 5$ on the depth–dose distribution along the isocentre, whereas the dose increment obtained by the PBA calculation was 51% lower than the measured increment (see figure 6).

Figure 9 compares the dose–area histograms obtained from the measurements and the PBA and PBRA calculations in each measurement plane.

The PBRA calculation was superior to the PBA, which underestimated the dose in deeper regions. The difference in calculation accuracy between the two algorithms arose from the consideration or disregard of irregular proton paths in heterogeneous media. The dose underestimation observed in the $Z = 4$ and $Z = 5$ planes even by the PBRA was caused by uncertainty in the CT value-to-range conversion and by the large low-density region. The doses in these regions are very sensitive to small uncertainties in the proton range because most protons in these regions have a small residual range. The reason for the large dose difference seen in the large dose gradient area is not well understood, but may be attributed to a lack of sufficient lateral scatter, which could be a result of a limitation of the redefinition process.

The trade-off between the calculation accuracy and computing time is often a significant factor in treatment planning. The computing time of the PBRA calculation was increased by the number of range bins, Rb (see m-loop in (11)), which depends on the complexity of the simulated geometry. For example, in the heterogeneous slab phantom, the number of range bins was up to three, owing to the L-shaped range compensator and the lateral heterogeneity (polyethylene/air). On the other hand, in the anthropomorphic phantom, up to 70 range bins were required for the PBRA calculation because of the complicated geometry. In the PBRA calculation, the slowing factors relative to the PBA calculation were 6.5 and 13.6 for the heterogeneity slab phantom and the anthropomorphic phantom, respectively. As shown in figure 8, the acceleration factors of the GPU-based acceleration of the PBRA calculation relative to the CPU-based PBRA calculation were 2.0 and 4.6 for the heterogeneity slab phantom and the anthropomorphic phantom, respectively. Fujimoto *et al* (2011) also found that GPUs were effective for implementing the PBA calculation. They observed 5–20 times faster performance using the NVIDIA Geforce GTX 480 card as compared to the Intel Core-i7

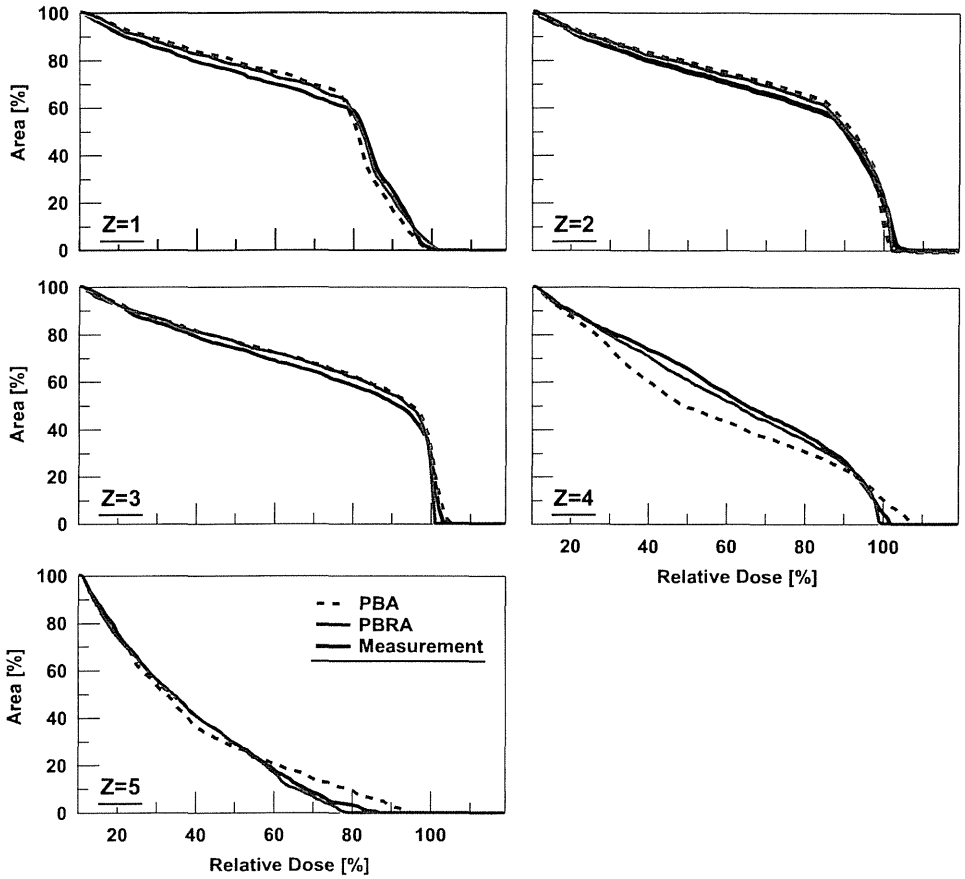

Figure 9. Dose–area histogram (DAH) at each measured plane.

920 processor. Their PBA, which employed 1D density scaling, used invariant dose kernelling, such that the data of the spatial variance of PB and the depth–dose distribution along the central axis of each PB could be stored in the GPU global memory before execution. In contrast, we used the Fermi–Eyges theory, in which the physics parameters were calculated and stored in the GPU global memory at each calculation plane. Because data transport between random access memory and GPU global memory can be a bottleneck of the GPU acceleration process (NVIDIA 2010), use of fewer accesses between the CPUs and GPUs may further accelerate the GPU-based PBRA calculation. Nevertheless, by the use of GPU implementation, dose calculation and optimization would help to reduce the clinical workload substantially in proton beam therapy.

5. Conclusions

The PBRA was applied to proton therapy to address the problem of lateral density heterogeneity. We addressed the problem of lateral density heterogeneity, by comparing the calculation results to dose distributions measured at different depths in a heterogeneous slab

phantom and an anthropomorphic phantom with a 2D detector. In the PBRA calculation, the redefined beams formed a detouring path that was different from the PBs without redefinition, and the path of each redefined beam was straight. Consequently, the PBRA was able to predict the measured proton-detouring effects. The GPU implementation of the PBRA achieved a speed-up factor of up to 4.6 relative to the PBRA calculation by CPU.

We conclude that the PBRA may improve the accuracy of PB calculation in heterogeneous media not only for electron therapy but also for proton therapy. The PBRA for protons requires more computational processes and longer computing time. However, by the use of GPU implementation, dose calculation and optimization would help to reduce the clinical workload substantially.

Acknowledgments

The authors would like to express their thanks to other members of the Medical Physics Group at NCCEH for their warm support and useful discussions. They also wish to thank SHI Accelerator Service, Ltd., for their help with measurements at the proton therapy facilities at the National Cancer Centre, Kashiwa. This work was partly supported by Health and Labour Science Research Grants from the Japanese Government. In addition, YE received a grant from the Japan Society for the Promotion of Science for Young Scientists as a Research Fellow of the Japan Society for the Promotion of Science.

Appendix. Statistical and phase-space parameters of the redefined beam

Statistical and phase-space parameters of the redefined beam on the z_p plane for mth range bin other than the number of particles $(N_{ij})_m$ and the mean residual range $(\overline{R}_{ij})_m$ are calculated in the same manner as the equation defined by Kanematsu *et al* (2008). The central axis position and the mean slopes of the redefined PBs are redefined at a patient plane $z = z_p$ as follows:

$$\left[\overline{x_{\mathrm{axis}ij}}\right]_m = x_j(z_p), \quad \left[\overline{y_{\mathrm{axis}ij}}\right]_m = y_i(z_p) \tag{A.1}$$

$$\left[\overline{a_{xij}}(z_p)\right]_m = \frac{1}{[N_{ij}(z_p)]_m} \sum_{kl} \sum_{\substack{n=1 \\ \epsilon R_m \leqslant (R^{\#}_{kl})_n < R_{m+1}}}^{R_h} \left(N^{\#}_{kl}\right)_n \cdot \mathrm{erfDiff}(y) \times \left\{\mathrm{erfDiff}(x) \cdot \left(\overline{a^{\#}_{xkl}}\right)_n - (A_{kl})_n \cdot \mathrm{expDiv}(x) \cdot \sinh \mathrm{Div}(x)\right\} \tag{A.2}$$

$$\left[\overline{a_{yij}}(z_p)\right]_m = \frac{1}{[N_{ij}(z_p)]_m} \sum_{k,l} \sum_{\substack{n=1 \\ \epsilon R_m \leqslant (R^{\#}_{i,j})_n < R_{m+1}}}^{R_h} \left(N^{\#}_{kl}\right) \cdot \mathrm{erfDiff}(x) \times \left\{\mathrm{erfDiff}(y) \cdot \left(\overline{a^{\#}_{ykj}}\right)_n - (A_{kl})_n \cdot \mathrm{expDiv}(y) \cdot \sinh \mathrm{Div}(y)\right\}. \tag{A.3}$$

Any parameter p at the plane immediately before the device is denoted as $p^{\#} = p(^{\#}z_p)$, where the PBs have not been redefined. erfDiff(x), expDiv(x), sinhDiv(x), coshDiv(x), $(A_{kl})_n$ appearing in the arguments of the function $\left[\overline{a_{xij}}(z_p)\right]_m$ and $\left[\overline{a_{yij}}(z_p)\right]_m$ are expressed as follows:

$$\mathrm{erfDiff}(x) \equiv \frac{1}{2}\left[\mathrm{erf}\left(\frac{(\Delta x^{\#})_n + \frac{\delta_{xy}}{2}}{\sqrt{2\left(\overline{t^{2\#}_{kl}}\right)_n}}\right) - \mathrm{erf}\left(\frac{(\Delta x^{\#})_n - \frac{\delta_{xy}}{2}}{\sqrt{2\left(\overline{t^{2\#}_{kl}}\right)_n}}\right)\right] \tag{A.4}$$

$$\mathrm{expDiv}(x) \equiv \exp\left(-\frac{(\Delta x^{\#})_n^2 + \frac{\delta_{xy}^2}{4}}{2\left(\overline{t^2}^{\#}_{kl}\right)_n}\right) \tag{A.5}$$

$$\sinh \mathrm{Div}(x) \equiv \sinh\left(\frac{(\Delta x^{\#})_n}{2\left(\overline{t^2}^{\#}_{kl}\right)_n} \cdot \delta_{xy}\right) \tag{A.6}$$

$$\cosh \mathrm{Div}(x) \equiv \cosh\left(\frac{(\Delta x^{\#})_n}{2\left(\overline{t^2}^{\#}_{kl}\right)_n} \cdot \delta_{xy}\right) \tag{A.7}$$

$$(A_{kl})_n \equiv \sqrt{\frac{2}{\pi\left(\overline{t_{kl}^2}^{\#}\right)_n^2}} \cdot \left(\overline{\theta t_{kl}}^{\#}\right)_n. \tag{A.8}$$

Similarly, the spatial variance $\left(\overline{t^2}_{ij}\right)_m$, angular variance $\left(\overline{\theta^2}_{ij}\right)_m$, and angular-spatial covariance $\left(\overline{\theta t}_{ij}\right)_m$ of the particles (Kanematsu *et al* 2008) are redefined as follows:

$$\left[\overline{\theta^2}_{ij}(z_p)\right]_m = \frac{1}{\left[N_{ij}(z_p)\right]_m} \sum_{kl} \sum_{\substack{n=1 \\ \epsilon R_m \leqq (R_{kl}^{\#})_n < R_{m+1}}}^{R_b} (N_{kl}^{\#})_n$$
$$\times \left\{ \begin{array}{l} \mathrm{erfDiff}(x) \cdot \mathrm{erfDiff}(y) \cdot \left(\left(\overline{\theta^2}^{\#}_{kl}\right)_n + \frac{[\overline{a_{x_{kl}}}^{\#}]_n^2 + [\overline{a_{y_{kl}}}^{\#}]_n^2}{2}\right) \\ -(B_{kl})_n \cdot \mathrm{expDiv}(x) \cdot \mathrm{erfDiff}(y) \\ \times \left[[E_{kl}(x)]_n \cdot \sinh \mathrm{Div}(x) + (D_{kl})_n \cdot \frac{\delta_{xy}}{4} \cdot \cosh \mathrm{Div}(x)\right] \\ -(B_{kl})_n \cdot \mathrm{expDiv}(y) \cdot \mathrm{erfDiff}(x) \\ \times \left[[E_{kl}(y)]_n \cdot \sinh \mathrm{Div}(y) + (D_{kl})_n \cdot \frac{\delta_{xy}}{4} \cdot \cosh \mathrm{Div}(y)\right] \end{array} \right\}$$
$$- \frac{[\overline{a}_{x_{ij}}(z_p)]_m^2 + [\overline{a}_{y_{ij}}(z_p)]_m^2}{2} \tag{A.9}$$

$$\left[\overline{\theta t}_{ij}(z_p)\right]_m = \frac{\delta_{xy}^2}{12\left|z_p - z_{\mathrm{src}}\right|}, \quad \left[\overline{t^2}_{ij}(z_p)\right]_m = \frac{\delta_{xy}^2}{12}. \tag{A.10}$$

$(B_{kl})_n$, $(D_{kl})_n$, $[E_{kl}(x)]_n$ appearing in the arguments of the function $\left[\overline{\theta^2}_{ij}(z_p)\right]_m$ are expressed as follows:

$$(B_{kl})_n \equiv \frac{\left(\overline{\theta t_{kl}}^{\#}\right)_n}{\sqrt{2\pi\left(\overline{t^2}^{\#}_{kl}\right)_n}} \tag{A.11}$$

$$(D_{kl})_n \equiv \frac{\left(\overline{\theta^2}^{\#}_{kl}\right)_n}{\left(\overline{t^2}^{\#}_{kl}\right)_n} \tag{A.12}$$

$$[E_{kl}(x)]_n \equiv \left[\overline{a_p}^{\#}_{kl}\right]_n - \frac{(\Delta x^{\#})_n}{2\left(\overline{t^2}^{\#}_{kl}\right)_n} \cdot \left(\overline{\theta t_{kl}}^{\#}\right)_n. \tag{A.13}$$

References

Boyd R A, Hogstrom K R and Starkschall G 2001 Electron pencil-beam redefinition algorithm dose calculations in the presence of heterogeneities *Med. Phys.* **28** 2096–104

Egashira Y, Nishio T, Matsuura T, Kameoka S and Uesaka M 2012 Experimental evaluation of a spatial resampling technique to improve the accuracy of pencil-beam dose calculation in proton therapy *Med. Phys.* **39** 4104

Eyges L 1948 Multiple scattering with energy loss *Phys. Rev.* **74** 1534–5

Fujimoto R, Kurihara T and Nagamine Y 2011 GPU-based fast pencil beam algorithm for proton therapy *Phys. Med. Biol.* **56** 1319–28

Gottschalk B, Koehler A M, Schneider R J, Sisterson J M and Wagner M S 1993 Multiple Coulomb scattering of 160 MeV protons *Nucl. Instrum. Methods* B **74** 467–90

Hogstrom K R, Michael M D and Almond P R 1981 Electron beam dose calculations *Phys. Med. Biol.* **26** 446–60

Hollmark M, Uhrdin J, Dž B, Gudowska I and Brahme A 2004 Influence of multiple scattering and energy loss straggling on the absorbed dose distributions of therapeutic light ion beams: I. Analytical pencil beam model *Phys. Med. Biol.* **49** 3247–65

Hong L, Goitein M, Bucciolini M, Comiskey R, Gottschalk B, Rosenthal S, Serago C and Urie M 1996 A pencil beam algorithm for proton dose calculations *Phys. Med. Biol.* **41** 1305

Hotta K, Kohno R, Takada Y, Hara Y, Tansho R, Himukai T, Kameoka S, Matsuura T, Nishio T and Ogino T 2010 Improved dose-calculation accuracy in proton treatment planning using a simplified Monte Carlo method verified with three-dimensional measurements in an anthropomorphic phantom *Phys. Med. Biol.* **55** 3545–56

Kanematsu N 2009a Semi-empirical formulation of multiple scattering for the Gaussian beam model of heavy charged particles stopping in tissue-like matter *Phys. Med. Biol.* **54** N67–73

Kanematsu N, Komori M, Yonai S and Ishizaki A 2009b Dynamic splitting of Gaussian pencil beams in heterogeneity-correction algorithms for radiotherapy with heavy charged particles *Phys. Med. Biol.* **54** 2015–27

Kanematsu N, Yonai S, Ishizaki A and Torikoshi M 2008 Computational modelling of beam-customization devices for heavy-charged-particle radiotherapy *Phys. Med. Biol.* **53** 3113–27

Kohno R, Takada Y, Sakae T, Terunuma T, Matsumoto K, Nohtomi A and Matsuda H 2003 Experimental evaluation of validity of simplified Monte Carlo method in proton dose calculations *Phys. Med. Biol.* **48** 1277–88

Kooy H M, Trofimov A, Engelsman M and Smith A R 2008 *Treatment planning Proton and Charged Particle Radiotherapy* ed T F Delaney and H M Kooy (Philadelphia, PA: Williams & Wilkins) chapter 8 pp 70–107

Nishio T 1999 Present status and planning of facilities for proton and heavy ion cancer treatment in Japan—National Cancer Center *J. At. Energy Soc. Japan* **41** 1134–8

Nishio T, Kataoka S, Tachibana M, Matsumura M, Uzawa N, Saito H, Sasano T, Yamaguchi M and Ogino T 2006 Development of a simple control system for uniform proton dose distribution in a dual-ring double scattering method *Phys. Med. Biol.* **51** 1249–60

NVIDIA 2010 NVIDIA CUDA Programming Guide Santa Clara, CA http://developer.download.nvidia.com/compute/cuda/3_0/toolkit/docs/NVIDIA_CUDA_ProgrammingGuide.pdf

Petti P L 1992 Differential-pencil-beam dose calculations for charged particles *Med. Phys.* **19** 137–49

Russell K R, Grusell E and Montelius A 1995 Dose calculations in proton beams: range straggling corrections and energy scaling *Phys. Med. Biol.* **40** 1031–43

Russell K R, Isacsson U, Saxner M, Ahnesjöh A, Montelius A, Grusell E, Vallhagen Dahlgren C, Lorin S and Glimelius B 2000 Implementation of pencil kernel and depth penetration algorithms for treatment planning of proton beams *Phys. Med. Biol.* **45** 9–27

Schaffner B, Pedroni E and Lomax A 1999 Dose calculation models for proton treatment planning using a dynamic beam delivery system: an attempt to include density heterogeneity effects in the analytical dose calculation *Phys. Med. Biol.* **44** 27–41

Shiu A and Hogstrom K R 1991 Pencil-beam redefinition algorithm for electron dose distributions *Med. Phys.* **18** 7–18

Spezi E, Angelini A L, Romani F and Ferri A 2005 Characterization of a 2D ion chamber array for the verification of radiotherapy treatments *Phys. Med. Biol.* **50** 3361–73

Szymanowski H, Mazal A, nauraye C, Biensan S, Ferrand R, Murillo M C, Caneva S, Gaboriaud G and Rosenwald J C 2001 Experimental determination and verification of the parameters used in a proton pencil beam algorithm *Med. Phys.* **28** 975–87

Szymanoqski H and Oelfke U 2002 Two-dimensional pencil beam scaling: An improved proton dose algorithm for heterogeneous media *Phys. Med. Biol.* **47** 3313–30

Tachikawa T, Sato T, Ogino T and Nishio T 1999 Proton treatment devices at National Cancer Center (Kashiwa, Japan) *Radiat. Indust.* **84** 48–53

Cancer Science
The official journal of the Japanese Cancer Association JCA

Long-term results of concurrent chemoradiotherapy using cisplatin and vinorelbine for stage III non-small-cell lung cancer

Hidehito Horinouchi,[1,6] Ikuo Sekine,[1] Minako Sumi,[2] Kazumasa Noda,[3] Koichi Goto,[4] Kiyoshi Mori[5] and Tomohide Tamura[1]

[1]Division of Internal Medicine and Thoracic Oncology, [2]Division of Radiation Oncology, National Cancer Center Hospital, Tokyo; [3]Department of Thoracic Oncology, Kanagawa Cancer Center, Yokohama; [4]Division of Thoracic Oncology, National Cancer Center Hospital East, Kashiwa; [5]Department of Medical Oncology, Division of Thoracic Oncology, Tochigi Cancer Center, Utsunomiya, Japan

(Received March 20, 2012/Revised September 9, 2012/Accepted September 13, 2012/Accepted manuscript online September 24, 2012/Article first published online November 8, 2012)

Concurrent chemoradiotherapy is the standard treatment for unresectable stage III non-small cell lung cancer (NSCLC). The long-term feasibility and efficacy of vinorelbine and cisplatin with concurrent thoracic radiotherapy were investigated. Eighteen patients received cisplatin (80 mg/m^2) on day 1 and vinorelbine (20 mg/m^2 in level 1, and 25 mg/m^2 in level 2) on days 1 and 8 every 4 weeks for four cycles in a phase I trial. Ninety-three patients received the same chemotherapy regimen except for the fixed vinorelbine (20 mg/m^2) dosage and consolidation therapy with docetaxel (60 mg/m^2, every 3 weeks). The thoracic radiotherapy consisted of a single dose of 2 Gy once daily to a total dose of 60 Gy. A total of 111 patients were analyzed in the present study: male/female, 91/20; median age, 60 years; stage IIIA/IIIB, 50/61; and squamous/non-squamous histology, 26/85. The 3-, 5-, and 7-year overall survival rates (95% CI) were 43.2% (33.9–52.2), 25.2% (17.6–33.5), and 23.2% (15.8–31.4), respectively. The median progression-free survival and median survival time (95% CI) were 13.5 (10.1–16.7) months and 30.0 (24.3–38.8) months, respectively. Four patients (4%) experienced Grade 5 pulmonary toxicities from 4.4 to 9.4 months after the start of treatment. In conclusion, approximately 15% of patients with unresectable stage III NSCLC could be cured with chemoradiotherapy without severe late toxicities after 10 months of follow-up. Although based on the data from highly selected population participated in phase I and phase II trial, this analysis would strengthen and confirm the previous reports concerning concurrent chemoradiotherapy with third generation cytotoxic agents. (*Cancer Sci* 2013; 104: 93–97)

Stage III locally advanced non-small cell lung cancer (NSCLC) accounts for 25–30% of all lung cancer cases.[1,2] Because of the equal frequency of local and distant recurrences, the combination of systemic chemotherapy and thoracic radiotherapy has been established as a standard of care for patients with stage III NSCLC.[3] Concurrent chemoradiotherapy is superior to a sequential approach, as shown by phase III trials in stage III NSCLC.[4,5]

Ohe *et al.*[6] reported the long-term follow-up analysis of concurrent chemoradiotherapy with former generation chemotherapy agents (median survival time 16.1 months, and 7-year overall survival rate 12.0%). Few researchers, however, have reported follow-up data of longer than 5 years after concurrent chemoradiotherapy with third-generation chemotherapy. The long-term safety and efficacy of vinorelbine and cisplatin with concurrent thoracic radiotherapy were investigated.

Materials and Methods

Study selection. Two previous studies were included in this analysis. One was a phase I study of concurrent thoracic radiotherapy with cisplatin plus vinorelbine, and the other evaluated docetaxel consolidation therapy following concurrent chemoradiotherapy.[7,8] These studies were approved by the institutional review board at each institution. Written, informed consent was obtained from all participating patients.

Patient selection. The two studies had similar eligibility criteria. They were: histologically or cytologically proven NSCLC; unresectable stage IIIA or IIIB disease; no previous treatment; measurable disease; tumor within an estimated irradiation field no larger than half the hemithorax; age between 20 years and 74 years; Eastern Cooperative Oncology Group (ECOG) performance status 0 or 1; and adequate organ function, including bone marrow, liver, kidney, and lung. Patients were diagnosed to have unresectable disease based on a consensus of thoracic oncologists including surgeons in each institution. The exclusion criteria were reported in previous papers.[7,8]

Treatment schedule. In the phase I study, treatment consisted of chemotherapy with four cycles of cisplatin and vinorelbine (20 mg/m^2 in level 1, and 25 mg/m^2 in level 2) and concurrent thoracic radiotherapy (see below). In the other study, treatment consisted of a chemoradiotherapy portion with three cycles of cisplatin and vinorelbine followed by a consolidation portion with three cycles of docetaxel. Cisplatin (80 mg/m^2) was administered every 4 weeks by intravenous infusion for 60 min with 2500–3000 mL of fluid for hydration. Vinorelbine 20 mg/m^2 diluted in 50 mL of normal saline was administered intravenously on days 1 and 8 every 4 weeks. All patients received prophylactic antiemetic therapy consisting of a $5HT_3$-antagonist and a steroid. In the docetaxel (60 mg/m^2, every 3 weeks) consolidation trial, consolidation therapy was started sequentially in patients whose general condition was acceptable. Follow-up computed tomographies after chemoradiotherapy were scheduled as follows; every 2–4 months during the 1 year, every 6 months in the 2 and 3 years, and every 1 year thereafter.

Thoracic radiotherapy was delivered with megavoltage equipment ($\geq$6 MV) using anterior/posterior opposed fields up to 40 Gy in 20 fractions, including the primary tumor, the metastatic lymph nodes, and the regional nodes. A booster dose of 20 Gy in 10 fractions was given to the primary tumor

[6]To whom correspondence should be addressed.
E-mail: hhorinou@ncc.go.jp

doi: 10.1111/cas.12028

and the metastatic lymph nodes for a total dose of 60 Gy using bilateral oblique fields. Computed tomography (CT) scan-based treatment planning was used in all patients. The clinical target volume (CTV) for the primary tumor was defined as the gross tumor volume (GTV) plus 1 cm taking into account subclinical extension. CTV and GTV for the metastatic nodes (>1 cm in the shortest dimension) were the same. Regional nodes, excluding the contralateral hilar and supraclavicular nodes, were included in the CTV, but the lower mediastinal nodes were included only if the primary tumor was located in the lower lobe of the lung. The planning target volumes for the primary tumor, the metastatic lymph nodes, and regional nodes were determined as CTVs plus 0.5–1.0-cm margins laterally and 1.0–2.0-cm margins craniocaudally, taking into account setup variations and internal organ motion. Lung heterogeneity corrections were not used.

Toxicity assessment. Toxicities were graded according to the National Cancer Institute (NCI) Common Toxicity Criteria version 2.0 issued in 1998, and late toxicities associated with thoracic radiotherapy were graded according to the Radiation Therapy Oncology Group/European Organization for Research and Treatment of Cancer late radiation morbidity scoring scheme.[9] Late toxicities were defined as those that occurred or persisted 90 days after completion of radiotherapy. The detailed methods of treatment modification due to toxicity were reported in previous papers.[7,8]

Response evaluation. In the phase I trial, the objective tumor response was evaluated according to the World Health Organization (WHO) criteria issued in 1979.[10] The Response Evaluation Criteria in Solid Tumors were used to evaluate objective tumor response in the docetaxel consolidation trial.[11] Local recurrences were defined as tumor progression in the primary site and in the hilar, mediastinal, and supraclavicular lymph nodes after a partial or complete response; regional recurrence was defined as the development of malignant pleural and pericardial effusions; and distant recurrence was defined as the appearance of distant metastases.

Statistical analyses. Progression-free and overall survival times were estimated by the Kaplan–Meier method, and confidence intervals (CIs) were based on Greenwood's formula.[12] Progression-free survival time was measured from the date of registration to the date of disease progression, death (from any cause), or the last follow-up. Overall survival time was measured from the date of registration to the date of death (from any cause) or to the last follow-up. Patients who were lost to follow-up without an event were censored at the date of their last known follow-up. A CI for response rate (RR) was calculated using methods for exact binomial CIs. To investigate the association between survival and factors related to patient characteristics, the Cox regression model was used. Potential factors investigated were as follows: age (in 10-year increments), sex, body weight loss ($\leq 5.0\%$ *vs* $\geq 5.1\%$), histology (squamous cell carcinoma versus non-squamous cell carcinoma), T factor (T1/2 *vs* T3/4), N factor (N0-2 *vs* N 3), and stage (IIIA *vs* IIIB). The STATA 10 for Windows software package (StataCorp LP, College Station, TX, USA) was used for statistical analyses.

Results

Characteristics of the patients. From October 1999 to June 2003, 13 patients were registered at dose level 1 and five at dose level 2 of the phase I study, and 93 patients were enrolled in the docetaxel consolidation trial. Thus, a total of 111 patients were analyzed in the present study. The participants' characteristics were as follows (Table 1): male/female 91/20; median age (range) 60 (31–74) years; body weight loss $\leq 5.0\%/\geq 5.1\%$ 96/14; stage IIIA/IIIB 50/61; and squamous/non-squamous histology 26/85.

Table 1. Patients' characteristics

	Clinical trial		
	Phase I trial†	DTX consolidation‡	Total
Number of patients	18	93	111
Age (years)			
Median	58.5	60	60
Range	48–69	31–74	31–74
Sex			
Male	15	76	91
Female	3	17	20
Performance status			
0	4	32	36
1	14	51	65
Unknown	0	10	10
Body weight loss (minus, %)			
0	11	72	83
0.1-5.0	4	9	13
5.1–	3	11	14
Unknown	0	1	1
Clinical stage			
IIIA	9	41	50
IIIB	9	52	61
N factor			
N0	0	6	6
N1	0	3	3
N2	11	58	69
N3	7	26	33
T factor			
T1	1	18	19
T2	6	31	37
T3	7	13	20
T4	4	30	34
Unknown	0	1	1
Histology			
Adenocarcinoma	14	57	71
Squamous cell carcinoma	3	23	26
Adenosquamous	1	0	1
Large cell carcinoma	0	6	6
NOS§	0	6	6
Others	0	1	1

†The phase I study of concurrent thoracic radiotherapy with cisplatin plus vinorelbine. ‡The docetaxel consolidation therapy following concurrent chemoradiotherapy study. §Non-small cell lung cancer not otherwise specified.

Treatment delivery. Full cycles (four in the phase I trial, three in the docetaxel consolidation trial) of cisplatin and vinorelbine and the full dose (60 Gy) of thoracic radiotherapy were administered in 94 (85%) and 102 (92%) patients, respectively. The delay in radiotherapy was less than 5 days in 74 (67%) patients. In the docetaxel consolidation trial, 59 (63%) patients could enter the consolidation phase, and only 34 (37%) patients completed three cycles of docetaxel chemotherapy, mainly because of toxicities. Of 91 patients with relapses, 27 (30%) received gefitinib as salvage treatments.

Objective tumor response and survival. The objective response rate was 82.0% (95% CI, 74.5–89.1). The 3-, 5-, and 7-year progression-free and overall survival rates (95% CI) were 21.0% (13.9–29.1), 15.7% (9.5–23.4), 14.4% (8.4–22.0), and 43.2% (33.9–52.2), 25.2% (17.6–33.5), and 23.1% (15.7–31.4), respectively (Fig. 1). The median progression-free survival and median survival time (95% CI) were 13.4 (9.8–16.4)

doi: 10.1111/cas.12028

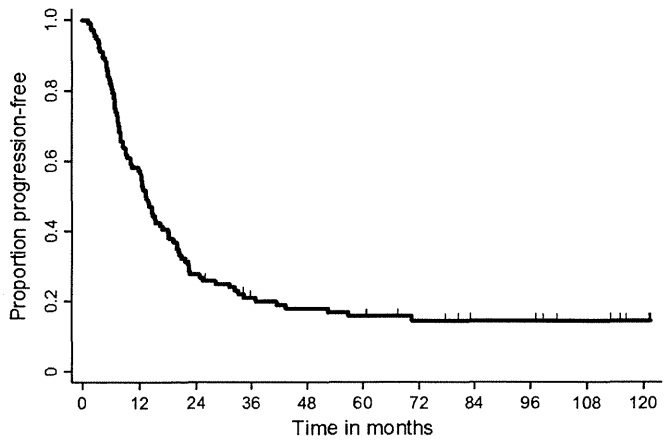

Fig. 1. Progression-free survival (n = 111). The median progression-free survival is 13.5 months (95% confidence interval [CI] 10.1–16.7).

months and 30.0 (24.5–38.8) months, respectively (Fig. 2). There was no significant difference in survival results between subgroups; patients with or without docetaxel consolidation and patients with or without gefitinib.

Pattern of relapse. Relapses were noted in 91 (82%) of 111 patients. Initial relapse sites were local alone in 39 (42%) patients, regional alone in 5 (5%), and distant alone in 38 (41%), including 17 (18%) patients with brain metastases as a sole recurrence site. Brain metastases were detected in 19 (21%) patients and were the most frequent sites of distant metastases. Brain metastases were detected within 3 years of initial treatment, and the last brain relapse was observed after 33 months of follow-up (Table 2). Three (3%) patients experienced adrenal metastases as a first relapse site.

Late toxicities. Grade 1, 2, 3, and 5 late pulmonary toxicities were observed in 18 (16%), 15 (13%), 3 (3%), and 4 (4%) patients, respectively. Seventy-two (64%) patients did not experience late pulmonary toxicities (Table 3). Four cases of grade 5 pulmonary toxicity developed at 4.4, 5.9, 9.4, and 9.6 months, respectively, after the treatment started. Late esophageal toxicities were observed in three patients (one grade 1 and two grade 3).

Causes of death in long-term survivors. There were 67 (60%) patients that survived 24 months or more from the initial treatment. Among them, five patients died because of reasons other

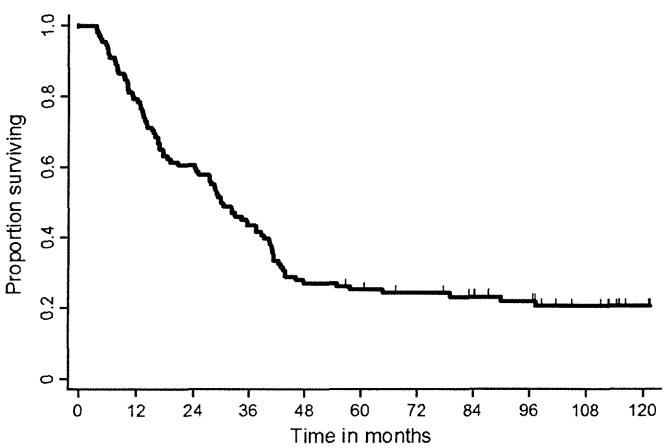

Fig. 2. Overall survival (n = 111). The median overall survival is 30.0 months (95% confidence interval [CI] 24.3–38.6).

Table 2. Sites of initial relapse

Site of recurrences	Number of relapses			
	<1 year	1–3 years	>3 years	Total (%)
Local	16	21	2	39 (42)
Distant	23	12	3	38 (41)
Distant without brain	12	4	3	19 (21)
Distant including brain	1	1	0	2 (2)
Brain only	10	7	0	17 (18)
Regional	3	2	0	5 (5)
Others (L/D/R)†	3	5	1	9 (10)
Unknown	–	–	–	2 (2)

†Others includes 2 Local+Regional relapses, 6 Local+Distant relapses, and 1 Local+Regional+Distant relapse.

Table 3. Late pulmonary toxicities§

Toxicity grades	Clinical trial		Total (%)
	Phase I trial†	DTX consolidation‡	
Without late toxicity	10	62	72 (64)
Grade 1	4	14	18 (16)
Grade 2	3	12	15 (13)
Grade 3	1	2	3 (3)
Grade 4	0	0	0
Grade 5¶	0	4	4 (4)

†The phase I study of concurrent thoracic radiotherapy with cisplatin plus vinorelbine. ‡The docetaxel consolidation therapy following concurrent chemoradiotherapy study. §Late toxicities were defined as those that occurred or persisted 90 days after completion of radiotherapy. ¶The Grade 5 pulmonary toxicities developed at 4.4, 5.9, 9.4, and 9.6 months after the treatment started.

than lung cancer. One patient was diagnosed as having pharyngeal cancer at the point of 35 months and died 4 months later. Other than malignancies, community-acquired pneumonia (one patient at 43 months), sudden death due to unknown etiology (two patients at 41 and 42 months) and suicide (one patient at 29 months) were reported, respectively.

Predictive factors for survival. The associations between overall survival and patients' characteristics (age [in 10-year increments], sex, body weight loss [$\leq 5.0\%$ *vs* $\geq 5.1\%$], histology [squamous cell carcinoma versus non-squamous cell carcinoma], T factor [T1/2 *vs* T3/4], N factor [N0-2 *vs* N 3], and stage [IIIA *vs* IIIB]) were also examined using Cox regression analysis. Age was significantly associated with survival (hazard ratio [HR] 1.34, 95% CI 1.02–1.75, Table 4).

Discussion

Concurrent chemoradiotherapy has been established as a standard treatment for patients with unresectable locally advanced NSCLC. The long-term feasibility and efficacy of vinorelbine and cisplatin chemotherapy with concurrent thoracic radiotherapy were investigated. The 3-, 5-, and 7-year overall survival rates (95% CI) were 43.2% (33.9–52.2), 25.2% (17.6–33.5), and 23.1% (15.7–31.4), respectively. Older age was associated with poor survival on multivariate analysis (HR 1.34, 95% CI 1.02–1.75).

Two phase III trial examined the efficacy and safety of newer generation cytotoxic agents in concurrent chemoradiotherapy for patients with locally advanced NSCLC.[13,14] The 5-year survival rates (around 20%) were comparable to cur-

Table 4. Cox proportional hazard model for assessment of overall survival

Factors	Hazard ratio	95% CI	*P* value
Age			
10-year increment	1		
	1.34	1.02–1.75	0.03
Sex			
Female	1		
Male	1.23	0.69–2.31	0.46
Body Weight Loss			
<5.0%	1		
>5.1%	1.19	0.69–2.11	0.51
Histology			
Non-squamous	1		
Squamous	1.31	0.80–2.19	0.28
T factor			
T1/2	1		
T3/4	0.91	0.53–1.61	0.77
N factor			
N 0–2	1		
N 3	1.05	0.55–2.08	0.85
Stage			
IIIA	1		
IIIB	0.97	0.52–1.83	0.93

rent analysis. To date, the present report (median survival time 30 months and 7-year overall survival rate 23.1%) is one of the longest observation periods after concurrent chemoradiotherapy using third-generation agents for locally advanced NSCLC. Recently, Tokuda *et al.*[15] reported a favorable long-term survival data (median survival time 2.1 years and 5-year survival rate 31%) of concurrent thoracic radiotherapy with docetaxel and cisplatin in a phase II trial conducted by Okayama Lung Cancer Study Group (OLCSG). It seems that the result of these analyses were about twice better than that of the previous long-term report of chemoradiotherapy with former generation agents by Ohe *et al.*[6] (median survival time 16.1 months and 7-year overall survival rate 12.0%) and others.[16]

Of the 91 patients with relapses, 85 (93%) experienced recurrence within 3 years after initial treatment. Local relapses (37 patients, 41%) and distant relapses (35 patients, 38%) were equally frequent. After 3 years of follow-up, two local, three distant (without brain), and one mixed-site recurrence was observed. Considering the proportion of local recurrence was similar to the OLCSG 0007 trial, a better strategy to control local relapse is a key to improving survival in locally advanced NSCLC.[13] To gain a better local control, the radiation therapy oncology group (RTOG) conducted a phase III trial (RTOG 0617) to examine a higher dose (74 Gy) of radiotherapy with concurrent chemotherapy. However, the experimental arms of higher radiotherapy were terminated early because of survival futility.[17] We recently reported early termination of a multicenter phase II trial of high-dose thoracic radiotherapy (72 Gy) because of slow accrual and pulmonary toxicities.[18] Based on these results, development of another strategy such as surgery followed by induction therapy might offer a better local control in selected patients.[19] On the other hand, 11 of 20 brain relapses as a first recurrence were found within a year of initial treatment. Several authors reported that brain metastases were frequent early in the course after the initial treatment of stage III NSCLC.[20,21] According to our findings and previous reports, intensive brain surveys might be indicated for such patients no longer than 3 years from initial chemoradiotherapy.

The frequency and control of late toxicities, especially lung injury, have been emphasized along with the improvement of survival by concurrent chemoradiotherapy in stage III NSCLC. In the present analysis, four patients (4%) in the docetaxel consolidation trial experienced grade 5 pulmonary toxicities 4.4–9.6 months from initial treatments. On the other hand, life-threatening pulmonary toxicities were not reported in phase I trial. (Table 3) This difference in the frequency of severe pulmonary toxicities might be related to consolidation docetaxel because the dose of cisplatin (80 mg/m^2), vinorelbine (20 mg/m^2) and thoracic radiotherapy (60 Gy) were the same in these two trials except for five patients who received 25 mg/m^2 of vinorelbine in the phase I trial.[7,8] A relatively higher frequency of pulmonary complications was also reported in the experimental arm of the previous phase III trial that examined docetaxel as a consolidation therapy after concurrent chemoradiotherapy.[22,23] Although a note of caution might be indicated with docetaxel, the present result suggests that severe pulmonary toxicities were rare after 10 months from concurrent chemoradiotherapy.

According to recent trials, about half of Japanese patients with locally advanced lung cancer survive more than 2 years after concurrent chemoradiotherapy.[13,14] In those who survived more than 2 years, mortalities due to second primary malignancies and etiologies other than lung cancer were reported by several authors.[15,24] Five patients (4.5%) died without recurrence of lung cancer and whose causes of death were as follows: second primary malignancy (pharyngeal cancer, one patient), community-acquired pneumonia (one patient), sudden death due to unknown etiology (two patients) and suicide (one patient), respectively. With an even greater proportion of patients cured by modern therapies including combined modality treatments, it would be increasingly important to consider and evaluate an appropriate care and monitoring for survivors.

In the present analysis, older age was significantly associated with poor survival (HR 1.34, 95% CI 1.02–1.75) after adjusting for sex, degree of weight loss, histology, T factor, N factor, and stage. In the previous literature on concurrent chemoradiotherapy with cisplatin and vinorelbine, age ($\geq$70 years) was marginally associated with poor survival (HR 1.79, 95% CI 0.94–3.39).[25] Several investigators reported higher incidences of adverse events in elderly patients with locally advanced NSCLC, even though they had a similar survival benefit.[26–28] Furthermore, better clinical outcomes were reported in elderly patients (>70 years) by thoracic radiotherapy rather than chemoradiotherapy with a similar regimen for younger patients.[29,30] Based on these reports, it is necessary to develop an optimal treatment strategy, especially to find the best chemotherapy regimen combined with thoracic radiotherapy, for elderly patients with stage III NSCLC.

This study had several limitations. First, the proportion of patients with stage IIIA disease was relatively high compared to previous phase III trials, which might have a favorable effect on overall survival.[13,14] Second, the population included in this analysis was relatively younger than those reported by Segawa *et al.*[13] and had better prognosis than real world patients. As discussed in this article, younger age might be a better prognostic factor in concurrent chemoradiotherapy (Table 3). The third limitation is potential selection bias in a highly selected population suitable for early phase clinical trials. To enable to follow clinical and prognostic information with the least missing data, however, we selected the patients that participated in the current phase I and feasibility trial of docetaxel consolidation.

doi: 10.1111/cas.12028

In conclusion, approximately 15% of patients with unresectable stage III NSCLC could be cured with chemoradiotherapy without severe late toxicities after 10 months of follow-up. Although based on the data from a highly selected population participated in phase I and phase II trial, this analysis would strengthen and confirm the previous reports concerning concurrent chemoradiotherapy with third generation cytotoxic agents.

Acknowledgement

We thank Ms Mika Nagai for her assistance in the preparation of this manuscript.

Disclosure Statement

The authors have no conflict of interest.

References

1 Mountain CF. Revisions in the International System for Staging Lung Cancer. *Chest* 1997; **111**: 1710–7.
2 Meerbeeck V. Staging of non-small cell lung cancer: consensus, controversies and challenges. *Lung Cancer* 2001; **34**: S95–107.
3 Jett JR, Scott WJ, Rivera MP, Sause WT. Guidelines on treatment of stage IIIB non-small cell lung cancer. *Chest* 2003; **123**: 221S–5S.
4 Furuse K, Fukuoka M, Kawahara M *et al.* Phase III study of concurrent versus sequential thoracic radiotherapy in combination with mitomycin, vindesine, and cisplatin in unresectable stage III non-small-cell lung cancer. *J Clin Oncol* 1999; **17**: 2692–9.
5 Fournel P, Robinet G, Thomas P *et al.* Randomized phase III trial of sequential chemoradiotherapy compared with concurrent chemoradiotherapy in locally advanced non-small-cell lung cancer: Groupe Lyon-Saint-Etienne d'Oncologie Thoracique-Groupe Francais de Pneumo-Cancerologie NPC 95-01 Study. *J Clin Oncol* 2005; **23**: 5910–7.
6 Ohe Y, Ishizuka N, Tamura T, Sekine I, Nishiwaki Y, Saijo N. Long-term follow-up of patients with unresectable locally advanced non-small cell lung cancer treated with chemoradiotherapy: a retrospective analysis of the data from the Japan Clinical Oncology Group trials (JCOG0003A). *Cancer Sci* 2003; **94**: 729–34.
7 Sekine I, Noda K, Oshita F *et al.* Phase I study of cisplatin, vinorelbine, and concurrent thoracic radiotherapy for unresectable stage III non-small cell lung cancer. *Cancer Sci* 2004; **95**: 691–5.
8 Sekine I, Nokihara H, Sumi M *et al.* Docetaxel consolidation therapy following cisplatin, vinorelbine, and concurrent thoracic radiotherapy in patients with unresectable stage III non-small cell lung cancer. *J Thorac Oncol* 2006; **1**: 810–5.
9 National Institutes of Health. *National Cancer Institute Common Toxicity Criteria, Version 2.0.* 1998. [Cited 30 Apr 1999.] Available from URL: http://ctep.cancer.gov/protocoldevelopment/electronic_applications/docs/ctcv20_4-30-992.pdf.
10 WHO. *Handbook for Reporting Results of Cancer Treatment.* Geneva: WHO Offset Publication, No. 48; 1979.
11 Therasse P, Arbuck SG, Eisenhauer EA *et al.* New guidelines to evaluate the response to treatment in solid tumors. European Organization for Research and Treatment of Cancer, National Cancer Institute of the United States, National Cancer Institute of Canada. *J Natl Cancer Inst* 2000; **92**: 205–16.
12 Armitage P, Berry G, Matthews J. Survival analysis. In: Armitage P, Berry G, Matthews J, eds. *Statistical Methods in Medical Research*, 4th edn. Oxford: Blackwell Science Ltd, 2002; 568–90.
13 Segawa Y, Kiura K, Takigawa N *et al.* Phase III trial comparing docetaxel and cisplatin combination chemotherapy with mitomycin, vindesine, and cisplatin combination chemotherapy with concurrent thoracic radiotherapy in locally advanced non-small-cell lung cancer: OLCSG 0007. *J Clin Oncol* 2010; **28**: 3299–306.
14 Yamamoto N, Nakagawa K, Nishimura Y *et al.* Phase III study comparing second- and third-generation regimens with concurrent thoracic radiotherapy in patients with unresectable stage III non-small-cell lung cancer: West Japan Thoracic Oncology Group WJTOG0105. *J Clin Oncol* 2010; **28**: 3739–45.
15 Tokuda Y, Takigawa N, Kozuki T *et al.* Long-term follow-up of phase II trial of docetaxel and cisplatin with concurrent thoracic radiation therapy for locally advanced non-small cell lung cancer. *Acta Oncol* 2012; **51**: 537–40.
16 Blackstock AW, Govindan R. Definitive chemoradiation for the treatment of locally advanced non small-cell lung cancer. *J Clin Oncol* 2007; **25**: 4146–52.
17 Bradley RP, Komaki R, Masters G *et al.* A Randomized Phase III Comparison of Standard-Dose (60 Gy) Versus High-dose (74 Gy) Conformal Chemoradiotherapy ± Cetuximab for Stage IIIA/IIIB Non-Small Cell Lung Cancer: Preliminary Findings on Radiation Dose in RTOG 0617. 53rd Annual Meeting of the American Society of Radiation Oncology 2011.
18 Horinouchi H, Sumi M, Satouchi M *et al.* Multicenter phase II study of concurrent high-dose (72Gy) three-dimensional conformal radiotherapy (3D-CRT) without elective nodal irradiation with chemotherapy using cisplatin and vinorelbine for unresectable stage III non-small cell lung cancer (NSCLC). ASCO annual conference. *J Clin Oncol* 2012; **30**: 7070.
19 Toyooka S, Kiura K, Takemoto M *et al.* Long-term outcome of induction chemoradiotherapy with docetaxel and cisplatin followed by surgery for non-small-cell lung cancer with mediastinal lymph node metastasis. *Interact Cardiovasc Thorac Surg* 2012; **14**: 565–9.
20 Gaspar LE, Chansky K, Albain KS *et al.* Time from treatment to subsequent diagnosis of brain metastases in stage III non-small-cell lung cancer: a retrospective review by the Southwest Oncology Group. *J Clin Oncol* 2005; **23**: 2955–61.
21 Horinouchi H, Sekine I, Sumi M *et al.* Brain metastases after definitive concurrent chemoradiotherapy in patients with stage III lung adenocarcinoma: carcinoembryonic antigen as a potential predictive factor. *Cancer Sci* 2012; **103**: 756–9.
22 Gandara DR, Chansky K, Albain KS *et al.* Consolidation docetaxel after concurrent chemoradiotherapy in stage IIIB non-small-cell lung cancer: Phase II Southwest Oncology Group Study S9504. *J Clin Oncol* 2003; **21**: 2004–10.
23 Hanna N, Neubauer M, Yiannoutsos C *et al.* Phase III study of cisplatin, etoposide, and concurrent chest radiation with or without consolidation docetaxel in patients with inoperable stage III non-small-cell lung cancer: the Hoosier Oncology Group and U.S. Oncology. *J Clin Oncol* 2008; **26**: 5755–60.
24 Takigawa N, Kiura K, Segawa Y *et al.* Second primary cancer in survivors following concurrent chemoradiation for locally advanced non-small-cell lung cancer. *Br J Cancer* 2006; **95**: 1142–4.
25 Naito Y, Kubota K, Nihei K *et al.* Concurrent chemoradiotherapy with cisplatin and vinorelbine for stage III non-small cell lung cancer. *J Thorac Oncol* 2008; **3**: 617–22.
26 Schild SE, Stella PJ, Geyer SM *et al.* The outcome of combined-modality therapy for stage III non-small-cell lung cancer in the elderly. *J Clin Oncol* 2003; **21**: 3201–6.
27 Schild SE, Mandrekar SJ, Jatoi A *et al.* The value of combined-modality therapy in elderly patients with stage III nonsmall cell lung cancer. *Cancer* 2007; **110**: 363–8.
28 Yuen AR, Zou G, Turrisi AT *et al.* Similar outcome of elderly patients in intergroup trial 0096: Cisplatin, etoposide, and thoracic radiotherapy administered once or twice daily in limited stage small cell lung carcinoma. *Cancer* 2000; **89**: 1953–60.
29 Movsas B, Scott C, Sause W *et al.* The benefit of treatment intensification is age and histology-dependent in patients with locally advanced non-small cell lung cancer (NSCLC): a quality-adjusted survival analysis of radiation therapy oncology group (RTOG) chemoradiation studies. *Int J Radiat Oncol Biol Phys* 1999; **45**: 1143–9.
30 Sause W, Kolesar P, Taylor SI *et al.* Final results of phase III trial in regionally advanced unresectable non-small cell lung cancer: Radiation Therapy Oncology Group, Eastern Cooperative Oncology Group, and Southwest Oncology Group. *Chest* 2000; **117**: 358–64.

Journal of Radiation Research, 2013, 54, 931–937
doi: 10.1093/jrr/rrt028 Advance Access Publication 4 April 2013

Radiation therapy for primary vaginal carcinoma

N. MURAKAMI[1,*], T. KASAMATSU[2], M. SUMI[1], R. YOSHIMURA[1], K. TAKAHASHI[1], K. INABA[1], M. MOROTA[1], H. MAYAHARA[1], Y. ITO[1] and J. ITAMI[1]

[1]Department of Radiation Oncology, National Cancer Center Hospital, 5-1-1, Tsukiji Chuo-ku, Tokyo 104-0045, Japan
[2]Department of Gynecologic Oncology, National Cancer Center Hospital, 5-1-1, Tsukiji Chuo-ku, Tokyo 104-0045, Japan
*Corresponding author. Tel: +81-3-3542-2511; Fax: +81-3-3545-3567; Email: namuraka@ncc.go.jp

(Received 9 December 2012; revised 4 March 2013; accepted 5 March 2013)

Brachytherapy plays a significant role in the management of cervical cancer, but the clinical significance of brachytherapy in the management of vaginal cancer remains to be defined. Thus, a single institutional experience in the treatment of primary invasive vaginal carcinoma was reviewed to define the role of brachytherapy. We retrospectively reviewed the charts of 36 patients with primary vaginal carcinoma who received definitive radiotherapy between 1992 and 2010. The treatment modalities included high-dose-rate intracavitary brachytherapy alone (HDR-ICBT; two patients), external beam radiation therapy alone (EBRT; 14 patients), a combination of EBRT and HDR-ICBT (10 patients), or high-dose-rate interstitial brachytherapy (HDR-ISBT; 10 patients). The median follow-up was 35.2 months. The 2-year local control rate (LCR), disease-free survival (DFS), and overall survival (OS) were 68.8%, 55.3% and 73.9%, respectively. The 2-year LCR for Stage I, II, III and IV was 100%, 87.5%, 51.5% and 0%, respectively ($P = 0.007$). In subgroup analysis consisting only of T2–T3 disease, the use of HDR-ISBT showed marginal significance for favorable 5-year LCR (88.9% vs 46.9%, $P = 0.064$). One patient each developed Grade 2 proctitis, Grade 2 cystitis, and a vaginal ulcer. We conclude that brachytherapy can play a central role in radiation therapy for primary vaginal cancer. Combining EBRT and HDR-ISBT for T2–T3 disease resulted in good local control.

Keywords: primary vaginal cancer; radiation therapy; high-dose-rate brachytherapy; intracavitary brachytherapy; interstitial brachytherapy

INTRODUCTION

The most common carcinoma affecting the vagina is metastatic from other primary gynecologic and non-gynecologic sites, including the cervix, endometrium, colon and rectum, ovary, and vulva. Primary vaginal cancer is considered to be a rare entity, accounting for only 2% of gynecologic malignancies [1, 2]. To diagnose primary vaginal cancer it is necessary to fulfill the following two conditions: the cervix and vulva must be free of disease [3]; and if a hysterectomy has been performed within five years for a uterine tumor, the histopathological findings must differ from that of the uterine tumor. Squamous cell carcinomas account for the majority of primary vaginal carcinomas. Other histological subtypes of vaginal carcinomas include adenocarcinoma, adenosquamous carcinoma, small cell carcinoma, melanoma, lymphoma and sarcoma. Most patients with vaginal carcinomas are in their sixth and seventh decades of life, with only 10% of cases occurring in patients ≤ 40 years of age; however, vaginal cancer is increasingly diagnosed in younger women, possibly because of human papillomavirus (HPV) infections [4].

There have been no prospective randomized trials with a focus on vaginal cancer treatments. Therefore, the management of vaginal cancer is not standardized, as is the treatment of cervical cancer. Small vaginal cancers, particularly those involving the apex of the vagina, may be treated successfully with surgical excision alone; however, definitive organ-sparing surgery is technically difficult for more advanced or distal lesions, which are usually treated with radiation therapy.

Before 2008, radiation therapy techniques applied to advanced primary vaginal cancer at the National Cancer Center Hospital in Tokyo, Japan, consisted of a combination of external beam radiation therapy (EBRT) and high-dose-rate intracavitary brachytherapy (HDR-ICBT), or EBRT

alone. After 2008, high-dose-rate interstitial brachytherapy (HDR-ISBT) was introduced. The purpose of this report is to retrospectively analyze the results of radiation therapy for primary vaginal cancer, and to determine whether or not the difference in radiation therapy technique affects disease control.

MATERIALS AND METHODS

The medical records of all patients treated with definitive radiation therapy for primary invasive carcinoma of the vagina at the National Cancer Center Hospital in Tokyo, Japan between February 1992 and November 2010 were reviewed retrospectively. Patients whose tumors involved the external os of the cervix or vulva were excluded [5]. Patients who had a hysterectomy for primary invasive uterine carcinoma with the same histology as vaginal cancer, patients who had distant metastases, and patients with histologic findings consistent with a sarcoma or melanoma were also excluded. Patients who had non-invasive carcinoma of the vagina, and patients who underwent EBRT post-operatively after hysterectomy for apical vaginal cancer, were excluded. A total of 36 patients with primary carcinoma of the vagina with a histopathological diagnosis of squamous cell carcinoma, adenocarcinoma, adenosquamous carcinoma and small cell carcinoma were included in this study.

All patients underwent a routine metastatic work-up, including a complete blood count, renal function testing, liver function testing, chest X-ray/CT, and pelvic CT/MRI. These patients were then evaluated jointly by gynecological oncologists and radiation oncologists for the purpose of staging and to determine the optimal treatment modality. Tumor size was determined by CT/MRI imaging. For superficial disease that could not be visualized with imaging studies, tumor size was determined by physical examination. With the exception of two patients who were treated by HDR-ICBT alone, the remaining 34 patients received EBRT. The common EBRT portals included the entire vagina, as well as the paracolpium, parametrium, and draining pelvic lymph nodes up to the level of the common iliac (L4/5 junction). If the primary lesion involved the lower one-third of the vagina or there were clinically palpable inguinal nodes, the inguinal regions were also included in the EBRT fields. Superficial tumors were treated by HDR-ICBT with or without EBRT. When HDR-ICBT was used in combination with EBRT, the treatment schedule was similar to the radiation therapy schedule for the treatment of cervical cancer in Japan [6, 7]. The initial 20–40 Gy was delivered to the whole pelvis, then pelvic irradiation with a central shield ensued. The total dose delivered to the pelvic side wall was up to 50 Gy using conventional fractionation. HDR-ICBT was delivered after pelvic irradiation with a central shield at 6–10 Gy/fraction to 5 mm under the vaginal surface, for a total of 2–5 fractions. Before 2008, HDR-ISBT was not used routinely in the treatment of vaginal cancer in our department. Advanced tumors that did not shrink sufficiently for HDR-ICBT after 40–50 Gy of pelvic irradiation were usually treated solely with EBRT with smaller boost fields of 60–70 Gy. For patients treated solely with EBRT, the median dose was 60 Gy (range, 49.6–70 Gy). For patients treated with a combination of EBRT and brachytherapy, the median EBRT dose for the central pelvis was 38 Gy (range, 20–50 Gy), the median EBRT dose for the pelvic side wall was 50 Gy (range, 36–50 Gy), the median ICBT dose was 18 Gy (range, 12–30 Gy), and the median ICBT dose per fraction was 6 Gy (range, 6–10 Gy). Of the two patients who were treated solely by ICBT, one patient was irradiated with 24 Gy in four fractions (6 Gy per fraction), and one patient was irradiated with 32 Gy in four fractions (8 Gy per fraction). After 2008, HDR-ISBT has been used routinely in the treatment of vaginal cancer in combination with EBRT. The detailed procedure for gynecological HDR-ISBT is described elsewhere [8]. In brief, a transperineal needle applicator insertion with transrectal ultrasound (TRUS) or CT image guidance was performed under general and epidural anesthesia or saddle block with the patient in the lithotomy position. After the needle applicator insertion, HDR-ISBT was performed twice daily, with each fraction 6 h apart. For advanced disease, a Syed-Neblett template^{TM} (Alpha Omega Services, Bellflower, CA, USA) was used to sufficiently cover lateral disease spread. For localized disease with limited paracolpium or parametrium invasion, free-handed needle applicator insertion with a vaginal applicator was used with fewer needles inserted compared with the Syed-Neblett template^{TM}. The gross target volume (GTV) was defined based on the CT image obtained after needle insertion, as well as on physical examination immediately before needle insertion, the intra-operative TRUS image, and the most recent MRI. The dwell time of Ir-192 and the dose distribution of HDR-ISBT was calculated by geometric optimization and graphical modification to enclose the GTV by the prescription dose. The median HDR-ISBT dose was 24 Gy (range, 22–32 Gy) and the median HDR-ISBT dose per fraction was 6 Gy (range, 4–6 Gy). HDR-ICBT and ISBT were performed with a MicroSelectron HDR^{TM} (Nucletron, Veenendaal, The Netherlands). Before 2010, administration of concurrent chemotherapy (cCRT) was not routinely used because there was no evidence that strongly favored utilization of cCRT for vaginal cancer; thus, the administration of cCRT was at the discretion of the attending physician and the most common agent used was cisplatin. After 2010, weekly cisplatin (40 mg/m^2) was used for bulky tumors (>4 cm) or patients with N1 disease, as is done for patients with cervical cancer.

After completion of radiotherapy, gynecological examinations were performed every 2–3 months for the initial

two years, every 4–6 months for years 3–5, and once or twice a year thereafter. Suspected persistent or recurrent disease was confirmed by a biopsy whenever possible. Treatment failures were classified as local, pelvic, or distant. Local failures were defined as persistent or recurrences located within the vagina or paracolpium. Pelvic failures were defined as recurrences in the pelvic or inguinal lymph nodes. Recurrences that involved the para-aortic nodes area were considered to be distant failures.

The local control rate (LCR), disease-free survival (DFS), and overall survival (OS) were calculated using the Kaplan Meier method [9] with all time intervals measured from the date of initiation of radiation therapy. The relationships between tumor characteristics and treatment variables, and LCR, DFS, and OS were analyzed by univariate analysis. The associations between tumor characteristics and treatment modality, and treatment modality and complications were evaluated with a chi-square test. A P-value < 0.05 was considered statistically significant. The continuous variables were dichotomized to give the lowest P-values in the log-rank test [10]. All statistical analyses were performed using SPSS™ (version 18.0; SPSS, Inc., Chicago, IL, USA).

This retrospective study was approved by the Institutional Review Board.

RESULTS

There were 36 patients who met the eligibility criteria; 24 patients were alive at the time of the analysis in May 2012 and 23 patients were free from loco-regional recurrence. The median follow-up length of all living patients and those who were treated by HDR-ISBT was 35.2 months (range, 12.3–151.3 months) and 29.3 months (range, 15.9–39.4 months), respectively. The pretreatment characteristics of the 36 patients are summarized in Table 1. The median age was 59 years (range, 25–94 years). Greater than one-half of the patients presented with T1 and T2 disease. Lymph node metastasis was noted in 10 patients. Five patients had undergone a hysterectomy for benign or non-invasive disease. Five patients had adenocarcinomas, one had an adenosquamous cell carcinoma, and one had a small cell carcinoma. The remaining 29 patients were diagnosed based on pathologic evaluation as squamous cell carcinoma. The median tumor size at diagnosis was 3.6 cm (range, 1.0–11 cm). Figure 1 shows the distribution of the initial tumor location in the vagina. The involvement of the upper one-third of the vagina and lateral wall involvement were most frequent (26/36 [72.2%] and 29/36 [80.6%], respectively). Table 2 shows the methods of treatment according to T classification. All patients with T1 disease were treated by brachytherapy with or without EBRT. No ICBT was applied for patients with T3–4 disease. Either EBRT alone or a combination of EBRT and ISBT was used for patients with T3 disease, while all patients with T4 disease were treated with EBRT alone. The tumor characteristics and treatment methods according to tumor histology are summarized in Table 3. Non-squamous cell carcinomas were more advanced compared with squamous cell carcinomas ($P = 0.006$, Table 3). Although there were no variables which were biased statistically because of the small number of patients, there was a tendency that non-squamous cell carcinomas was treated more frequently by EBRT alone than squamous cell carcinomas.

The 2-year LCR, DFS and OS were 68.8%, 55.3% and 73.9%, respectively. The 2-year LCR was 100% for Stage I, 87.5% for Stage II, 51.5% for Stage III, and 0% for Stage IV ($P = 0.007$, Table 1). The LCR was significantly unfavorable for patients with a non-squamous cell carcinoma histologic diagnosis (81.9% vs 14.3%, $P < 0.001$). In T2–T3 patients, in which EBRT alone or a combination of EBRT and HDR-ICBT/ISBT was used, HDR-ISBT had a marginally favorable LCR (88.9% vs 46.9%, $P = 0.064$, Fig. 2). In another analysis of the T1–T3 patients who had received EBRT and HDR-ICBT/ISBT, the 2-year LCR for EBRT + HDR-ICBT and EBRT + HDR-ISBT was identical (90%; $P = 0.970$). As shown in Table 1, the treatment result was not influenced by the treatment period (before or after 2008), when HDR-ISBT was introduced routinely for advanced disease.

Of the 36 patients in the current study, 17 (47.2 %) had persistent disease or recurrences; Fig. 3 shows the sites of initial failure of the 17 patients. Local recurrence was the most frequent site of recurrence.

One patient developed Grade 2 proctitis 8 months after radiation therapy and one patient developed Grade 2 cystitis 36.4 months after radiation therapy. Vaginal complications were assessed for 23 patients who did not have loco-regional recurrences (Table 4). Vaginal adhesions were noted in nine patients and were the most frequent complication; however, most of the adhesions were lysed with manual manipulation. Two patients each had vaginal atresia and strictures. A vaginal ulcer developed in one patient 17.3 months after radiation therapy, and healed with conservative treatment. No vesicovaginal or rectovaginal fistulae formed, and no patients with hemorrhagic cystitis required a blood transfusion. As shown in Table 4, the correlation between vaginal complications and administration of brachytherapy was analyzed using a chi-square test; the incidence of vaginal complications was not influenced by brachytherapy; rather there was a trend that patients treated with EBRT alone were more likely to develop vaginal adhesions ($P = 0.056$, Table 4). One patient developed a sacral bone fracture 11 months after radiation therapy.

DISCUSSION

Carcinoma of the vagina is a rare gynecological malignancy that primarily affects the elderly. Because of the

Table 1. Patient, tumor and treatment characteristics and correlation with outcome

Characteristic	*n* (%)	2-year LCR (%)	*P*	2-year DFS (%)	*P*	2-year OS (%)	*P*
Age							
<60	18 (50)	77.8	0.343	55.6	0.848	72.2	0.811
≥60	18 (50)	60		55		76.2	
Previous hysterectomy							
yes	5 (13.9)	60	0.416	60	0.928	60	0.456
no	31 (86.1)	70.3		54.6		76.2	
Stage							
I	9 (25)	100	0.007*	80	0.003*	100	0.053
II	8 (22.2)	87.5		75		62.5	
III	17 (47.2)	51.5		29.4		69.1	
IV	2 (5.6)	0		0		0	
T-Stage							
T1	9 (25)	100	0.013*	80	0.03*	100	0.051
T2	13 (36.1)	76.9		46.2		59.8	
T3	12 (33.3)	48.6		41.7		73.3	
T4	2 (5.6)	0		0		0	
N-Stage							
N0	26 (72.2)	68.5	0.804	64.9	0.062	68.4	0.071
N1	10 (27.8)	70		30		60	
Histology							
Scc	29 (80.6)	81.9	<0.001*	68.6	<0.001*	82.1	0.01*
non-Scc	7 (19.4)	14.3		0		42.9	
Tumor size							
<4 cm	20 (55.6)	80	0.133	65	0.241	74.1	0.758
≥4 cm	16 (44.4)	54.7		43.8		74	
Brachytherapy (HDR-ICBT/ISBT)							
yes	22 (61.1)	90.9	0.001*	77.3	0.001*	86.4	0.008*
no	14 (38.9)	32.1		21.4		53	
HDR-ISBT (T2–T3)							
yes	9	88.9	0.064	55.6	0.313	88.9	0.196
no	18	46.9		36.5		52.1	
Concurrent chemotherapy							
yes	7 (19.4)	64.3	0.773	28.6	0.298	71.4	0.472
no	29 (80.6)	69		62.1		74.3	
Treated period							
before 2008	23 (63.9)	60.2	0.178	51.8	0.561	68.6	0.2
after 2008	13 (36.1)	84.6		61.5		83.9	

LCR = local control rate, DFS = disease-free survival, OS = overall survival, HDR-ICBT = high-dose-rate intracavitary brachytherapy, HDR-ISBT = high-dose-rate interstitial brachytherapy.